Spatial Transformer for 3D Point Clouds

Jiayun Wang, Rudrasis Chakraborty, and Stella X. Yu

Abstract—Deep neural networks can efficiently process the 3D point cloud data. At each layer, the network needs to partition points into multiple local patches, and then learn features from them, in order to understand the geometric information encoded in the 3D point cloud. Previous networks adopt all the same local patches for different layers, as they utilized the same fixed original 3D point coordinates to define local neighborhoods. It is easy to implement but not necessarily optimal. Ideally local patches should be different at different layers so as to adapt to the specific layer for efficient feature learning. One way to achieve this is to learn different transformations of the original point cloud at each layer, and then learn features from local patches defined on transformed coordinates. In this work, we propose a novel approach to learn different non-rigid transformations of the input point cloud for different local neighborhoods at each layer. We propose both linear (affine) and non-linear (projective and deformable) spatial transformer for 3D points. With spatial transformers on the ShapeNet part segmentation dataset, the network achieves higher accuracy for all categories, specifically with 8% gain on earphones and rockets. The proposed methods also outperform the state-of-the-art methods in several other point cloud processing tasks (classification, semantic segmentation and detection). Visualizations show that spatial transformers can learn features more efficiently by altering local neighborhoods according to the semantic information of 3D shapes regardless of variations in a category.

Index Terms—point cloud, transformation, segmentation, 3D detection

______ **+** ______

INTRODUCTION

ECENT years have witnessed the emergence and increasing popularity of 3D computer vision techniques to understand the 3D world, with the development of 3D sensors and technology. An efficient way to model the 3D world is using 3D sensors such as depth cameras, LiDAR etc.. These 3D sensors can output 3D point cloud, which is a key component in several 3D computer vision tasks including but not limited to virtual/ augmented reality [1], [2], 3D scenes understanding [3], [4], [5], and autonomous driving [6], [7], [8].

Convolutional neural networks (CNNs) have achieved great success in many computer vision tasks [9], [10]. However, CNNs cannot be directly applied to analyze the 3D point cloud for 3D vision, because of the irregular neighborhood around each point. An obvious step to overcome this bottleneck is to convert the point cloud into a representation where applying CNNs is meaningful. Several researchers tackled this problem either by converting the 3D point cloud into regular voxel representation [11], [12], [13] or using view projection [14], [15], [16], [17].

More recently, network architectures [18], [19], [20], [21] that directly work on 3D point clouds have been developed. Analogous to the CNNs, given a set of points, the point "convolution layer" will need to find "local patch" around each input point using the point affinity matrix (affinity matrix is defined as the adjacency matrix of the dense graph constructed from the point cloud). This local patches are then used to extract local features using convolutions defined on points. By stacking the basic point convolution layers, the network can extract information from point clouds at different levels. Nonetheless, unlike images where local patches are well-defined, defining local patches for 3D point clouds is not simple. The local patches should cope with

complicated geometric transformation in 3D shapes. In most methods [18], [19], [22], [23], the local patches have been defined by using nearest neighbors of the original 3D coordinates in standard euclidean distance.

The usage of euclidean-distance based nearest neighbor search on the same 3D coordinates may be simple but not optimal, as (a) Euclidean distance may not be sufficient to capture geometric transformations of different 3D shapes; (b) Different layers usually target at different levels of information, and fixed nearest neighbor graph constrains the changes at different abstract level.

In order to alleviate above-mentioned problems, we propose to dynamically learn the point affinity matrix to find local patches. In order to dynamically learn the affinity matrix, we will use both point coordinates and learned feature maps. At different layers of the network, we propose to learn several different transformation graphs (dubbed as *spatial transformers* hereafter, Fig. 1) and corresponding point local neighborhood (Fig. 2). Spatial transformers enable the possibility of the network to learn different point cloud features within different "local patches". In the remainder of this section, we will briefly describe our approach to dynamically learn the local neighborhood and summarize our main contributions.

In order to transform point clouds for defining local patches, a straightforward approach is to learn a function, Φ , to generate new point set coordinates from the original point set location and current feature map. However, without any constraint on Φ , learning such a function is not easy. An alternative way is to put a smoothness constraint on the function Φ . Observe that any isometric transformation (e.g. rigid) can not change the topology. Hence, in this work, we will use non-rigid transformations, including linear/affine and non-linear transformations to model Φ . In other words, we will learn "spatial transformers" using the point cloud coordinates, P, and feature map, F, to generate new point clouds for building new affinity matrix. Then, we can find

The authors are with UC Berkeley / ICSI, 1947 Center St, Berkeley, CA, 94704. E-mail: {peterwg, rudra, stellayu}@berkeley.edu.

[•] Our code us publicly available at http://pwang.pw/spn.html.

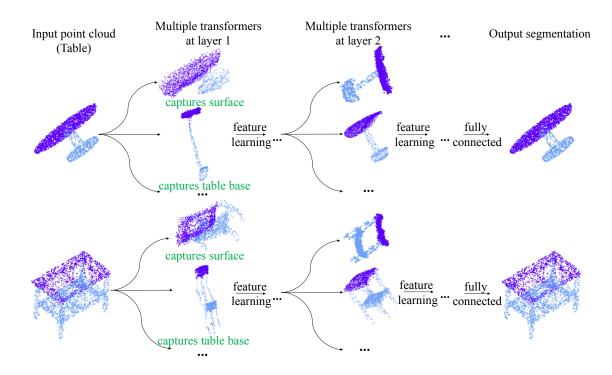


Fig. 1. From 3D point clouds to semantics. We propose spatial transformers on point clouds that can be easily added to existing point cloud processing networks. The transformer learns class-specific transformations for point cloud, build affinity matrix (usually based on k-NN graph), derive local patches, and then apply point convolutions. Corresponding transformers capture similar geometric transformations regardless of the sample variations in a category. Different parts of 3D tables are marked in different colors for visual aid, and are not fed to networks.

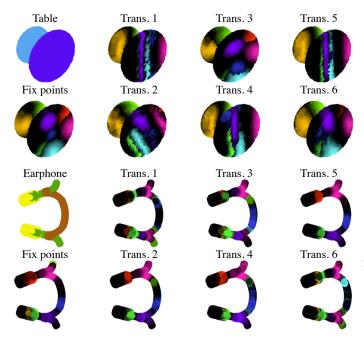


Fig. 2. **Nearest neighbor retrieval** of several query points using (transformed) 3D coordinates. Previous works use static local neighborhood of points with the same original 3D coordinates at different layers. We proposed to learn multiple different spatial transformers at different layers to have different local patches. Rotating table and earphone for better visualizations.

local patches based on the adaptive affinity matrix (usually k-NN measured by ℓ_2 distance).

We learned the spatial transformations using multiple

schemes: (a) affine spatial transformation $P\mapsto AP$, where A is an affine matrix. (b) projective spatial transformer $\widetilde{P}\mapsto B\widetilde{P}$, where, \widetilde{P} is in the homogeneous coordinates. (c) deformable spatial transformer $P\mapsto CP+DF$ as nonlinear transformation, where C,D are respective transformation matrices of point coordinates and features, and P is a combination of transformed point coordinates and features.

In summary, our main contributions are: (a) We propose linear (affine) and non-linear (projective, deformable) spatial transformers for 3D point clouds for learning affinity matrix and in-turn local patch. (b) We demonstrate that the proposed spatial transformers can be easily added to the existing point cloud networks for different tasks (classification, segmentation and detection). (c) We apply the proposed spatial transformers to different types of point cloud processing networks (point-based and sampling-based), and observe improved performance compared to its fixed graph (using the same original coordinate based affinity matrix) counterpart.

2 RELATED WORKS

In this section, we discuss some related works to motivate the necessity of our proposed framework.

View-based and voxel-based networks. View-based methods project 3D shapes to 2D plane and use a group of images from different views as the representation. Taking advantages of the power of CNNs in 2D image processing [24], [25], [15], [14], view-based methods have achieved reasonable 3D processing performance. Yet, the geometric shape information get lost when projecting from 3D to 2D.

Representing 3D shapes as volumetric data based on regular 3D grid, and processing with 3D convolution have

also been adopted by many works [11], [26], [27]. However, the quantization artifacts, the inefficient use of the 3D voxels and low resolution due to computation capacity highly limits the volumetric methods. Furthermore, 3D convolution usually performs away from the surface, and cannot capture sufficient 3D shape information. Recent works that applied different partition strategies [28], [12], [27], [13] somehow relieved such issues but still depended on bounding volume subdivision, instead of fine-grained local geometric shape. On the contrary, our work directly take 3D point cloud as input to minimize geometric information loss and to maximize the processing efficiency.

Point cloud processing networks. Some deep neural networks directly take point cloud as input and learn semantic/ abstract information by point processing operations. As a pioneering work, PointNet [18] directly learned embedding of every isolated 3D points and gather that information by pooling point features later on. Although achieving reasonable accuracy, PointNet did not learn any local geometric information of the 3D shape. PointNet++ relieved this by proposing a hierarchical application of isolated 3D point feature learning to multiple subsets of point cloud data. Many other works also explored different strategies in leveraging local structure learning of point cloud data [22], [23]. Instead of finding neighbors of each point, SplatNet [29] encoded local structure from sampling perspective: it grouped points based on permutohedral lattices [30], and then applied bilateral convolution [31] for feature learning. Super-point graphs [32] proposed to partition point cloud into superpoints and learned the 3D point geometric organization. Most of the works focus on learning local geometric information from given 3D point "local patches" [19], [29], [23], few of them provide insights on how to form the "local patches".

Point cloud is defined in an irregular grid, and regular convolution operation cannot be directly applied. Many works [22], [23], [33] aimed at designing point convolution operation, which resembles image convolution, for point cloud data. However, most work directly used original input point cloud to find the local patches for the convolution operation. As 3D shapes has diverse geometric transformations, and efficient learning requires the point convolution operation to be invariant to such transformations. Fixed 3D shape in all layers as the input to find local patches greatly limits the network's flexibility in handling this issue. In contrast, our work propose spatial transformers on the point cloud to capture geometric transformations in a more adaptive/ flexible and efficient way.

3 METHODS

In this section, we briefly review different geometric transformation methods and their influence on the affinity matrix of point cloud data, followed by the design of our three spatial transformers, namely, (a) affine, (b) projective and (c) deformable. We can apply the spatial transformer block, consisting of multiple spatial transformers, to each layer of a network for altering local patches for better point feature learning. We conclude the section by introducing how the transformers can be added to existing point cloud processing networks and the relevance to other works.

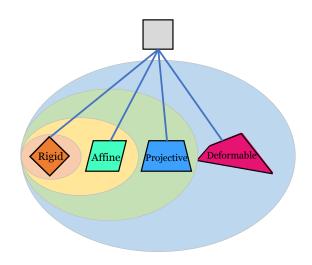


Fig. 3. **Different geometric transformations.** We illustrate how a grey square transforms after rigid, affine, projective and deformable transformations.

3.1 Geometric Transformations

We propose to learn transformations on the original point cloud to "deform" the original geometric shape, and build new affinity matrices based on graph constructed using k nearest neighbors (k-NN). The learned affinity matrix will deform the local patches (constructed using ℓ_2 distance) to ease the feature learning from the deformed local patch. The hypothesis behind the usage of geometric transformation is as follows:

Hypothesis 1. Let $P = \{\mathbf{p}_i\}$ be the input point cloud and let \mathcal{N}_i be "the" local neighborhood (patch) around $\mathbf{p}_i \in \mathbf{R}^3$ from which we are extracting local feature. Let $\mathcal{N} = \{\mathcal{N}_i\}$ be the set of local patches. Assume $\widetilde{\mathcal{N}} = \{\widetilde{\mathcal{N}}_i\}$ be the "optimal" neighborhood for learning local features, then $\exists (smooth) \ \Phi : \mathcal{N}_i \to \widetilde{\mathcal{N}}_i$ for all \mathbf{p}_i .

Essentially we are going to use different types of geometric transformations to approximate Φ . The new learned affinity matrix will dynamically alter the "local patch" to allow more representative feature learning.

As in Fig. 3, transformations can be categorized into rigid and non-rigid transformations, and non-rigid transformations can be further partitioned into linear and non-linear transformations. We briefly review different transformation methods below.

Rigid transformations: The group of rigid transformations consist of translations and rotations. However, rigid transformations are isometric (in ℓ_2 distance) and therefore preserves the affinity matrix. Thus, local patches are "invariant" to rigid transformations in terms of k-NN graph. Hence, we do not consider this transformations in this paper.

Affine transformations: The affine transformation is the non-rigid linear transformation. Consider a 3D point cloud $P = \{\mathbf{p}_i\}_{i=1}^N \subset \mathbf{R}^3$ consists of N three-dimensional vectors $\mathbf{p}_i \in \mathbf{R}^3$. Then, an affine transformation can be parameterized by an invertible matrix $A \in \mathbf{R}^{3\times3}$ and a translation vector $\mathbf{b} \in \mathbf{R}^3$. Given A, \mathbf{b} , we will get the affine transformed coordinate of \mathbf{p}_i as $\mathbf{p}_i \mapsto A\mathbf{p}_i + \mathbf{b}$. Note that translation \mathbf{b} will not change the k-NN graph. Recall that, an affine transformation preserves collinearity, parallelism and convexity.

Projective transformations: The projective transformation (or homography) is a non-rigid non-linear transformation. We first map the 3D point sets P to the homogeneous space and get \widetilde{P} , i.e., we concatenate ones as the last dimension. The projective transformation is parameterized by $A \in \mathbf{R}^{4\times 4}$ and we get the transformed point as $\widetilde{\mathbf{p}}_i \mapsto A\widetilde{\mathbf{p}}_i$. Compared to the affine transformations, projective transformations have more degrees of freedom but cannot preserve parallelism.

Deformable transformations: When all the points have the freedom to move without much constraint, the 3D shape can deform freely. We refer to it as the deformable transformation. This transformation has more degrees of freedom and does not preserve the topology. We learn deformable transformation from both point locations and features, as described in the following subsection.

3.2 Spatial Transformers for 3D Point Clouds

We can apply a geometric transformation to the given point cloud to obtain different local patches for feature learning, which we dub as *spatial transformer*. Our spatial transformers can be applied to existing point cloud processing networks as transformers will only alter "local patches". We briefly introduce our affine, projective and deformable spatial transformers as follows.

Suppose at layer t, the spatial transformer block contains $k^{(t)}$ spatial transformers. Each transformer will learn a transformation on the input point coordinates (we refer to the transformed points as sub-graph) first and calculate the corresponding sub-feature. Finally we concatenate all sub-features of each transformer to form the final feature output of the learning block. Suppose the i^{th} spatial transformer at t^{th} layer takes as input the original point cloud $P \in \mathbf{R}^{3 \times N}$ and previous feature map $\mathcal{F}^{(t-1)} \in \mathbf{R}^{f^{(t-1)} \times N}$.

Affine: We form $k^{(t)}$ new transformed point from \mathbf{p}_j as:

$$\mathbf{g}_{i,j}^{(t)} = A_i^{(t)} \mathbf{p}_j + \mathbf{b}_i^{(t)}, \quad i = 1, 2, ..., k^{(t)}.$$
 (1)

As the affinity matrix is invariant under uniform scaling and translation, we set $\|A_i\|_F=1, b=0$, for all i. Thus, we can simplify Equation 1 as follows:

$$G_i^{(t)} = A_i^{(t)} P, \quad i = 1, 2, \cdots, k^{(t)},$$
 (2)

where, $G_i^{(t)} = \left\{\mathbf{g}_{i,j}^{(t)}\right\}_j$. We will apply k-NN in each transformed point $G_i^{(t)}$ to obtain the affinity matrix $S_i^{(t)}$. For every affinity matrix $S_i^{(t)}$, we can define local patches for point clouds and thus do point convolution operation on previous point cloud feature map $\mathcal{F}^{(t-1)}$ and get the point cloud feature $F_i^{(t)} \in \mathbf{R}^{f_i^{(t)} \times N}$ of the sub-graph, referring to one transformation and its corresponding altered neighborhood:

$$F_i^{(t)} = \mathsf{CONV}(\mathcal{F}^{(t-1)}, S_i^{(t)}, k), \quad i = 1, 2, ..., k^{(t)}, \quad \ \ (3)$$

where, CONV is the point convolution operation: it takes (a) previous point cloud feature, (b) affinity matrix (for defining local patch of each point) and (c) number of neighbors (for defining the size of local patches) as input. In some point convolution operations (such as [22]), the affinity matrix will alter the input feature in a non-differentiable way. Thus, we

concatenate the transformed point cloud $P_i^{(t)}$ to the input feature for the sake of back-propagation of transformation matrix A. In some sampling-based convolution operations (such as bilateral convolution [29]), affinity matrix will change the input feature in a differentiable way, therefore no additional operation is needed.

For all the $k^{(t)}$ sub-graph in layer/ block t, we can learn $k^{(t)}$ point cloud features $F_i^{(t)}$. The output of this learning module will be the concatenation of all the sub-graph point cloud features:

$$\mathcal{F}^{(t)} = \mathsf{CONCAT}(F_1^{(t)}, F_2^{(t)}, ..., F_{k^{(t)}}^{(t)}), \tag{4}$$

where, $F_i^{(t)} \in \mathbf{R}^{f_i^{(t)} \times N}$ and $\mathfrak{f}^{(t)} = \sum_i^{k^{(t)}} f_i^{(t)}$, $\mathcal{F}^{(t)} \in \mathbf{R}^{\mathfrak{f}^{(t)} \times N}$. In our implementation, we randomly initialize A from standard normal distribution, i.e., $\mathcal{N}(0,1)$. Before computing the coordinate of the transformed point cloud, we normalize the transformation matrix, A by the norm $\|A\|_F$, to quotient out the uniform scaling as the affinity matrix is invariant under uniform scaling.

Projective: Analogous to the affine spatial transformers, for the i^{th} graph at t^{th} layer, we first apply projective transformation to the point cloud \widetilde{P} in homogeneous coordinates and get the transformed point cloud as:

$$\widetilde{G}_{i}^{(t)} = B_{i}^{(t)} \widetilde{P}, \quad i = 1, 2, \cdots, k^{(t)},$$
 (5)

where, $B_i^{(t)} \in \mathbf{R}^{4 \times 4}$ is the transformation matrix in the homogeneous coordinates.

We then follow the same point cloud feature learning as defined in Equation 3, and concatenate them as in Equation 4 to get output feature \mathcal{F}^t of the t^{th} layer.

Deformable: Affine and projective transformations are useful in transforming the original point cloud data, altering the affinity matrix, and providing learnable "local patch" for point convolution operation at different layers. Nonetheless, the ability to transform the affinity matrix and in turn the local patches is limited as affine transformations are linear mapping. Although "projective transformation" has more flexibility than affine in the sense parallelism is not preserved, the restriction that "projective transformation" maps a straight line to a straight line makes it not general enough to capture all possible deformations. To alleviate this problem and capture more geometric transformation of the point cloud, we propose a non-linear spatial transformer - deformable spatial transformer.

The deformable transformation at t^{th} layer and i^{th} subgraph can be written as:

$$G_i^{(t)} = A_i^{(t)} P + D_i^{(t)},$$
 (6)

where, $A_i^{(t)}P$ is the affine transformation, and deformation matrix $D_i^{(t)} \in \mathbf{R}^{3 \times N}$ gives every point the freedom to move, so the geometric shape of the whole point cloud has the flexibility to deform. Note that the translation vector \mathbf{b} in Equation 1 is a special case of the deformation matrix $D_i^{(t)}$, and in general the deformation matrix $D_i^{(t)}$ can significantly change the local patch.

As a self-supervised learning procedure, the spatial transformer parameters are learned from both point cloud coordinates and features. Since affine transformation $A_i^{(t)}P$

can capture the location (coordinate) information, we use deformation matrix $D_i^{(t)}$ to capture feature map changes given by $D_i^{(t)} = \mathcal{C}_i^{(t)} \mathcal{F}^{(t-1)}$, where, $\mathcal{F}^{(t-1)} \in \mathbf{R}^{\mathfrak{f} \times N}$ is the feature map of previous layer, $\mathcal{C}_i^{(t)} \in \mathbf{R}^{3 \times \mathfrak{f}}$ transforms the feature from $\mathbf{R}^{\mathfrak{f}}$ to \mathbf{R}^3 . Hence, the deformable transformation in Equation 6 can be simplified as:

$$G_i^{(t)} = \begin{bmatrix} A_i^{(t)} & \mathcal{C}_i^{(t)} \end{bmatrix} \begin{bmatrix} P \\ \mathcal{F}^{(t-1)} \end{bmatrix} = C_i^{(t)} \begin{bmatrix} P \\ \mathcal{F}^{(t-1)} \end{bmatrix}, \quad (7)$$

where, $C_i^{(t)} \in \mathbf{R}^{3 \times (3 + f^{(t-1)})}$ is the concatenation of affine and deformable transformation matrix that captures both point cloud location and feature map projection.

After we compute the transformed point location $G^{(t)}$, we will follow the Equations 3 and 4 to learn the feature of each sub-transformation graph, and concatenate them as the final output feature of layer t.

For the deformable spatial transformer, we decompose the entire transformation in two parts: $A_i^{(t)}P$ and $\mathcal{C}_i^{(t)}\mathcal{F}^{(t-1)}$. The former is the affine transformation of point 3D coordinates, while the latter is a transformation of the point feature. The transformation of point spatial location captures the linear transformation information of the point cloud, and the feature transformation captures the relatively high-level semantic information. The deformable transformation sums the two sources of information together. In Section 4.5, we provide empirical analysis of these two components.

3.3 Spatial Transformer Networks

Spatial transformers discussed above aim to dynamically transform the point cloud and change the local patches for point convolution operation. The transformer can be easily added to existing point cloud processing networks. We introduce how a general point cloud processing network with spatial transformers work, and then provide three applications in different networks and tasks as examples.

Point cloud processing networks with spatial transformers. We take point cloud segmentation task as an example, Fig. 4 depicts a general network architecture for this task. Suppose it is a C class segmentation task with the input point cloud in \mathbb{R}^3 consisting N points. Our network consists of several spatial transformers at different layers. At layer t, we learn $k^{(t)}$ transformation matrices $\{A_i^{(t)}\}_{i=1}^{k^{(t)}}$ to apply on the original point cloud coordinates P, and compute the corresponding affinity matrices $\{S_i^{(t)}\}_{i=1}^{k(t)}$ (e.g. based on k-NN graphs in the edge convolution [22] for point cloud). For each sub-transformation, we can learn a feature $F_i^{(t)}$ of dimension $N \times f_i^{(t)}$; then we concatenate all $k^{(t)}$ features in this layer to form an output feature \mathcal{F}^t of dimension $N \times \mathfrak{f}^{(t)}$, where $\mathfrak{f}^{(t)} = \sum_i^{k^{(t)}} f_i^{(t)}$. The output feature serves as the input of the next layer for further feature learning. Note that since different layer can have multiple spatial transformers, the affine/ projective transformation matrix will only be applied on the original point cloud coordinates P. Specifically for deformable transformation, deformable matrix $C_i^{(t)}$ applies on previous feature map, thus the feature transformation component is progressively learned. By stacking several such transformation learning blocks and finally a fully connected layer of dimension C, we can map the input point cloud to the segmentation map of dimension $C \times N$, or downsample to vector of dimension C for classification task. We can train the network end-to-end with some modern optimization methods. For spatial transformer block in point cloud detection network (Fig. 5), C is dimension of the output feature.

Applications in Classification Networks. Point cloud classification networks [19], [23] take point clouds as input, learn features from local patches and finally output classifier of dimension C, where C is the number of classes. We add spatial transformer blocks at each layer to obtain different local patches for feature learning.

Applications in Point-based Segmentation Networks. Point-based segmentation networks [19], [18], [23], [22] take point clouds as input and derive affinity matrix and local patches from the point locations. For selected points, certain "convolution" operators on the points and its local patches will be applied to learn the feature map. We choose edge convolution from [22] as our baseline which takes relative point location as input and achieves state-of-theart performance. Specifically, we retain all the setting of the method, just insert the spatial transformers to provide new local patches for the edge convolutional operation.

Applications in Sampling-based Segmentation Networks. SplatNet [29] is a representative of sampling-based segmentation networks. It also takes point clouds as input, but use permutohedral lattice [30] to group points into lattices and performs learned bilateral filters [31] on the grouped points to get feature. The permutohedral lattice defines the local patches of each points to make the bilateral convolution possible. We use spatial transformers to deform the point clouds and form new permutohedral lattices on the transformed point sets. The local patches can therefore dynamically cope with the geometric shape of the point cloud. All the other components in SplatNet remains the same.

Application in Detection Networks. Object detection in 3D point clouds is an important problem in many applications, such as autonomous navigation, housekeeping robots, and AR/ VR. LiDAR point cloud, as the one of the most popular sensory data for 3D detection, is usually highly sparse and imbalanced. The proposed spatial transformers specializes in transforming the point clouds for dynamic local patches, and has the potential of processing LiDAR data efficiently. We use VoxelNet [34], which achieves the state-ofthe-art performance in 3D object detection in autonomous driving data, as our baseline model. As in Fig. 5, we follow all the settings in VoxelNet, but add spatial transformers on the raw point cloud data, before point grouping. The spatial transformer feature learning blocks only change point feature but not the point location for grouping. It can be considered as improving the point cloud learning process.

3.4 Relevance to Other Works

The idea of spatial transformer has much relevance to some previous work. We briefly review its relevance to deformable CNN [35] and DGCNN [22].

Relevance to Deformable CNN. Deformable convolutional networks [35] propose to learn dynamic local patches for 2D image. Specifically for each location \mathbf{p}_0 on the output

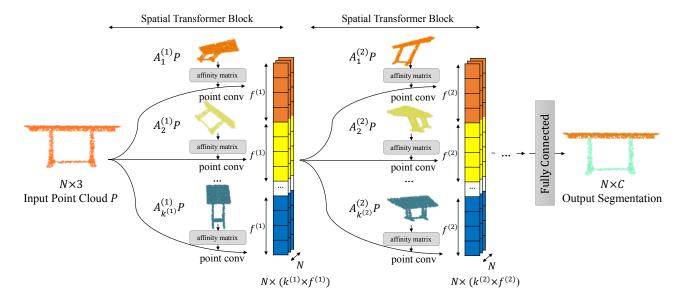


Fig. 4. The point cloud segmentation network with spatial transformers. Our network consists of several spatial transformers. At each layer, we learn k transformation matrices A to apply on the original point cloud P, and compute the corresponding affinity matrices based on k-NN graph. For each sub transformation, we can learn a sub-feature, and then concatenate all features to form an output feature of dimension $f \times N$. The output feature will be used for the next spatial transformer block for feature learning. By stacking several such transformation learning blocks and finally a fully connected layer of dimension C (the number of class), we can map the input point cloud to the $C \times N$ segmentation map.

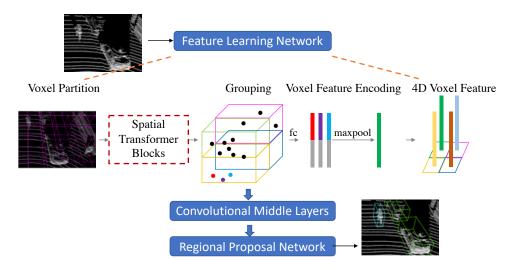


Fig. 5. **Object detection network** based on [34]. We add spatial transformer blocks to obtain dynamic local patches for the point feature learning network.

feature map Y, deformable convolution augments the regular grid R with offsets $\{\Delta \mathbf{p_n}\}_{n=1}^N$, where N=|R|. Then the convolutional output on input X parameterized by weight \mathbf{w} becomes:

$$Y(\mathbf{p_0}) = \sum_{\mathbf{p_n} \in \mathbf{R}^3} w(\mathbf{p_n}) X(\mathbf{p_0} + \mathbf{p_n} + \Delta \mathbf{p_n})$$
(8)

The offset augmentation to the regular grid R is very similar to the deformable transformation (Equation 6): we also want to give each point the freedom to move. For 2D images (matrices) defined in regular grid, the dynamic grid is necessary to model geometric transformation [35]. For 3D point clouds defined in irregular grid, the dynamic grid is also necessary to model even more complicated 3D geometric transformation.

Relevance to Dynamic Graph CNN. The idea of having dynamic local patches on point cloud processing has also been explored in DGCNN [22]. We summarize the difference of their idea and our work as follows: (a) For point convolution operation, they directly reuse the high-dimensional feature map from the previous layer, to construct dynamic graph for affinity matrix and local patches. Reusing point feature to build affinity matrix blurs the boundary between spatial and semantic information and may not be optimal; (b) It is not easy to build dense nearest neighbor graph in high-dimensional feature space; (c) DGCNN [22] only have one graph at different layers. At each layer, we transform both point cloud location and feature as in Equation 7 to ${\bf R}^3$ to compute the affinity matrix and in-turn construct the local patches. We also have multiple graphs at each layer

to deform the point cloud differently, in order to capture different geometric transformations. With less computation burden and more flexibility in geometric transformations, we demonstrate better empirical performances as shown in two semantic segmentation experiments (Section 4.2 and 4.3.)

4 EXPERIMENTS

In this section, we arrange comprehensive experiments to verify the effectiveness of the proposed spatial transformer. First, we evaluate the transformer on two types of networks (point-based and sampling-based) for four point cloud processing tasks (classification, part segmentation, semantic segmentation and detection). We then conduct ablation studies on the deformable spatial transformer. We conclude this section with visualization, analysis and insights on the proposed method.

4.1 Classification

We report the performance of our spatial transformers on the ModelNet40 3D shape classification dataset [11]. We evaluate on two baseline methods [22], [29] and adopt the same network architecture, experimental setting and evaluation protocols. We show that adding the spatial transformer to point-based and sampling-based method gives 1% and 2% gain on ModelNet40 (Table 4.1 and Fig. 6).

As in Fig. 10, spatial transformers can align the global 3D shape better according to its semantic meaning, we would ask "Can spatial transformers still align shapes even with random rotation?" To verify this, we augment both the training and testing data with random rotation, and observe that the spatial transformer gives 3% gain over its fix graph counterpart.

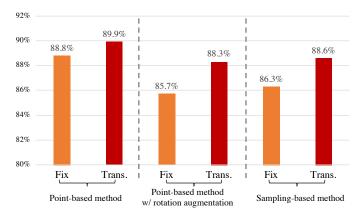


Fig. 6. Classification accuracy on ModelNet40. "Trans." refers to our deformable spatial transformer. We observe accuracy gain of every baseline networks with spatial transformers.

4.2 Part Segmentation

3D point cloud part segmentation is an important yet challenging fine-grained 3D analysis task - given a 3D point cloud, the task aims at accurately assigning the part category label (e.g. chair leg, cup handle) to each point. We evaluate the proposed modules on ShapeNet part segmentation dataset [36]. The dataset contains 16,881 shapes from 16

categories, annotated with 50 parts in total, with number of parts per category from ranges from 2 to 6. On each sample, ground truth has been annotated.

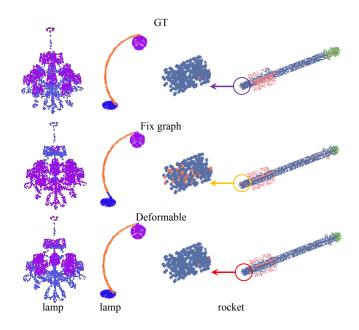


Fig. 7. Qualitative results for part segmentation of deformable spatial transformers. We observe better segmentation result with spatial transformers.

4.2.1 Point-based Method

Network architectures. Point-based segmentation networks take point clouds as input and derive affinity matrix and construct local patches from the point location, for defining "convolution" operation on points. We use the state-of-the-art point-based segmentation networks, Dynamic graph CNN (DGCNN) [22]. We follow the same network architecture and evaluation protocol. Specifically this work uses "edge convolution" as the point convolution operation. The network has 3 convolutional layers, with output feature dimension of 64. Additionally, in order to capture different level information of the input point clouds, they concatenate all the convolutional features and use several fully connected layers to map the feature to the final segmentation output.

We insert our spatial transformer to alter the local patch definition for edge convolution operation. We first use the original point cloud location and name it *fixed graph* baseline. With the affine, projective and deformable spatial transformer defined in Section 3.2, we also have point-based *affine*, *projective* and *deformable* networks. Specifically DGCNN directly used learned feature to build affinity matrix (based on *k*-NN graph) to obtain local patches, and we consider this as point-based *dynamic graph* network.

Under the framework of 3 edge convolution layers, we kept number of graphs in each layer k and sub-graph feature dimension f the same, and search for the best architecture. Due to memory limitation, we report the affine, projective and deformable network with k=4, f=32 at the best performance. To make fair comparison, we also increase the # of channels of fixed-graph baseline and dynamic networks.

Result and analysis. In Table 4.2.1, we report instance average mIOU (mean intersection over union), as well as

TABLE 1
Classification accuracy on ModelNet40 dataset.

]	Point-base	d	Point-based (R) Sampling base			sed	
		PointNet [18]	DGCNN [22]	[22] (fixed)	Affine	Deformable	[22] (fixed)	Deformable	SplatNet[29]	Affine	Deformable
Ī	Avg.	86.2	89.2	88.8	89.3	89.9	85.7	88.3	86.3	87.4	88.6

'R' denotes both training and testing data augmented with random rotations. We observe accuracy gain of every baseline networks with spatial transformers.

the mIOU of some representative categories in ShapeNet. Compared with the fixed graph baseline, the affine, projective and deformable spatial transformers respectively achieve 0.5%, 0.2% and 1.1% improvement and beats the fixed graph baseline methods in most categories. Specifically, we observe 8.0%, 8.3% and 4.7% performance boost in deformable spatial transformers compared with the fixed graph baseline. Compared with the dynamic graph network, the deformable spatial transformers improve by 4.0%. We also beat other state-of-the-art methods [18], [19], [20] by a significant margin. We also add deformable spatial transformers on PointCNN [23] and observe 6% and 4% gain on motorbike and bag, as well as 1% gain on average. Fig. 7 qualitatively visualize some part segmentation results of the fixed graph baseline our deformable spatial transformer. Deformable spatial transformer makes the prediction more smooth and achieves better performance, compared with the fixed graph baseline.

From affine to projective, and to deformable transformers, the performance increases as the level of freedom goes up. Projective spatial transformer, however, seems to have similar or worse performance than affine, and we believe the mapping to homogeneous may inhibit the ability to capture geometric transformation. When the freedom further improves and we directly use learned features as input to define affinity matrix and find local patches (dynamic-graph), yet the performance drops. We believe the need for both point location and feature to learn the affinity matrix, rather than reusing the high-dimensional point cloud features.

4.2.2 Sampling-based Method

Sampling-based point cloud processing methods group 3D points first, and then conduct convolution on the grouped points. SplatNet [29], as a representative method, applies permutohedral lattice [30] to group points into lattices and performs learned bilateral filters [31] on the grouped points to extract feature. In comparison, the bilateral convolution operates on the grouped points, and enjoys the advantages of naturally defined local neighbors at different direction.

Network architecture. We follow the same architecture as SplatNet [29]: the network starts with a single 1×1 regular convolutional layer, followed by 5 bilateral convolution layers (BCL). The output of all BCL are concatenated and feed to a final 1×1 regular convolutional layer to get the segmentation output. Since each BCL directly takes raw point cloud location as input, we consider it as fixed graph baseline. We add deformable spatial transformer to the networks and feed transformed point graphs to BCL to construct the permutohedral lattice. Because of the gradient to the permutohedral lattice grid, we can make the transformation matrix learned end-to-end. Note that we increase the channel of convolution layers for fair comparison.

Result and analysis. We report the performance of deformable spatial transformer (with k=1 at all BCLs) in Table 4.2.1. Compared with sampling-based fixed graph baseline [29], the deformable module achieves 0.6% improvement and performance boost in most categories (improves 5.9% for rocket). Deformable spatial transformer also beats other state-of-art baselines.

4.3 Semantic Segmentation

Semantic segmentation for point cloud data is a challenging but has high practical significance, such as for robotic vision. The task is similar to part segmentation, only point labels become semantic object classes instead of part labels.

We conduct experiments on the Standford 3D semantic parsing dataset [37]. The dataset contains 3D scans from Matterport scanners in 6 areas including 271 rooms. Each point in the scan is annotated with one of the semantic labels from 13 categories (chair, table, floor etc. plus clutter).

We follow the data processing procedure of [18] for Stanford 3D Indoor Scenes Dataset [37]. Specifically, we first splits points by room, and then sample rooms into several $1m \times 1m$ blocks. When training, 4096 points are sampled from the block on the fly. We train our network to predict per point class in each block, where each point is represented by a 9 dimensional vector of XYZ, RGB and normalized location (in the range of (0, 1)) as to the room.

Network architectures. The network architecture is based on DGCNN [22]. The network architecture is the same as Section 4.2, with the dimension C of final segmentation label changes to 13.

Result Analysis. In Table 4.3, we report the performance of the affine and deformable spatial transformer networks, and compare with our fixed graph baseline and several other state-of-the-art methods. Compared with our fixed graph baseline, affine spatial transformer achieves 0.9% average mIOU improvement, while deformable achieves 1.2% average mIOU improvement. Specifically compared with the dynamic graph [22], the deformable spatial transformer is also 1.1%. Our deformable spatial transformer beats all other state-of-the-art methods. Similarly for sampling-based methods [29], we observe 1.4% average mIOU improvement.

From the result, we have similar conclusion as in the part segmentation experiments: when given point clouds more freedom to the to deform (from affine to deformable spatial transformer) based on transformation of original location and feature projection, the segmentation performance improves. However, when directly using high-dimensional point feature to find affinity matrix, the performance drops due to lack of regularization.

Fig. 9 depicts qualitative results for semantic segmentation of our deformable transformation learning module. Our network is able to output smooth predictions and is robust to missing points and occlusions.

TABLE 2
Part segmentation results on ShapeNet PartSeg dataset. Metric is mIoU(%) on points.

	Avg.	aero	bag	cap	car	chair	earphone	guitar	knife	lamp	laptop	motorbike	mug	pistol	rocket	skateboard	table
# shapes		2690	76	55	898	3758	69	787	392	1547	451	202	184	283	66	152	5271
3DCNN [18]	79.4	75.1	72.8	73.3	70.0	87.2	63.5	88.4	79.6	74.4	93.9	58.7	91.8	76.4	51.2	65.3	77.1
PointNet[18]	83.7	83.4	78.7	82.5	74.9	89.6	73.0	91.5	85.9	80.8	95.3	65.2	93.0	81.2	57.9	72.8	80.6
PointNet++ [19]	85.0	82.4	79.0	87.7	77.3	90.8	71.8	91.0	85.9	83.7	95.3	71.6	94.1	81.3	58.7	76.4	82.6
FCPN [20]	81.3	84.0	82.8	86.4	88.3	83.3	73.6	93.4	87.4	77.4	97.7	81.4	95.8	87.7	68.4	83.6	73.4
DGCNN [22]	81.3	84.0	82.8	86.4	78.0	90.9	76.8	91.1	87.4	83.0	95.7	66.2	94.7	80.3	58.7	74.2	80.1
Point-based [22] fixed graph	84.2	83.7	82.4	84.0	78.2	90.9	69.9	91.3	86.6	82.5	95.8	66.5	94.0	80.8	56	73.8	79.8
Point-based affine	84.7	84.1	83.5	86.9	79.6	90.9	72.5	91.6	88.2	83.3	96.1	68.9	95.3	83.3	60.9	75.2	79.7
Point-based projective	84.4	84.3	84.2	88.5	77.9	90.4	72.8	91.2	86.6	81.7	96.0	66.6	94.8	81.3	61.6	72.1	80.5
Point-based deformable	85.3	84.6	83.3	88.7	79.4	90.9	77.9	91.7	87.6	83.5	96.0	68.8	95.2	82.4	64.3	76.3	81.5
PointCNN [23]	84.9	82.7	82.8	82.5	80.0	90.1	75.8	91.3	87.8	82.6	95.7	69.8	93.6	81.1	61.5	80.1	81.9
PointCNN deformable	85.8	83.4	86.6	85.5	79.1	90.3	78.5	91.6	87.8	84.2	95.8	75.3	94.6	83.3	65.0	80.7	81.7
Sampling-based baseline [29]	84.6	81.9	83.9	88.6	79.5	90.1	73.5	91.3	84.7	84.5	96.3	69.7	95.0	81.7	59.2	70.4	81.3
Sampling-based deformable	85.2	82.9	83.8	87.6	79.6	90.6	73.0	92.2	86.1	85.7	96.3	72.7	95.8	83.1	65.1	76.5	81.3

Compared with several other methods, our method achieves the SOTA in average mIoU.

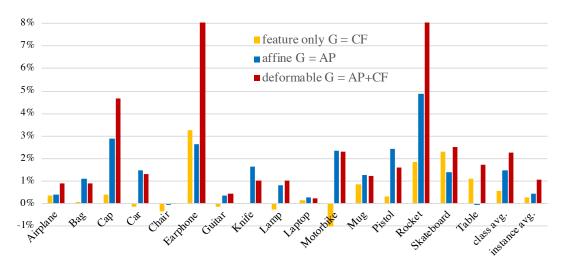


Fig. 8. **Performance improvement** on ShapeNet part segmentation task (compared to fixed graph) of different components of deformable spatial transformers. Our deformable spatial transformers achieves gain on every category, specifically with 8% gain on earphone and rocket.

TABLE 3
Semantic segmentation results on S3DIS semantic segmentation dataset. Metric is mIoU(%) on points.

	PointNet[18]	DGCNN[22]	[22](FIXED)	[22]+AFF	[22]+DEF	SplatNet [29]	[29]+DEF
	47.7	56.1	56.0	56.9	57.2	54.1	55.5
	ceiling	floor	wall	beam	column	window	clutter
[22](FIXED)	92.5	93.1	76.1	51.0	41.7	49.6	46.8
[22]+AFF	92.7	93.6	76.7	52.6	41.2	48.7	47.8
[22]+DEF	92.8	93.6	76.8	52.9	41.1	49.0	48.0
	door	table	chair	sofa	bookcase	board	
[22](FIXED)	63.4	61.8	43.1	23.3	42.0	43.5	
[22]+AFF	63.7	63.4	45.1	27.0	41.3	44.8	
[22]+DEF	63.5	64.2	45.2	28.1	41.7	46.1	

Compared with other methods, our method outperforms the SOTA in avg. mIoU.

TABLE 4
Detection results on KITTI validation set (car class). Metric is AP(%) on points.

		birds' eve			3D			
	Easy	Medium	Hard	Easy	Medium	Hard		
VoxelNet[34]	77.3	59.6	51.6	43.8	32.6	27.9		
VoxelNet + fixed graph	84.3	67.2	59.0	45.7	34.5	32.4		
VoxelNet + deformable	85.3	69.1	60.9	46.1	35.9	34.0		

Adding our spatial transformers improves the performance by around 2%.

4.4 3D Object Detection

We also explore how the proposed methods performs in point cloud detection. We evaluate on the KITTI 3D object detection

benchmark [38] which contains 7,481 training images/point clouds and 7,518 test images/point clouds, covering three categories: Car, Pedestrian, and Cyclist. For each class, detection outcomes are evaluated based on three difficulty levels: easy, moderate, and hard, which are determined according to the object size, occlusion state and truncation level. We follow the evaluation protocol in VoxelNet [34] and report the car detection result on the validation set.

Network architecture. As shown in Fig. 5, the network takes raw point clouds as input and partition the points based into voxels. We add deformable spatial transformer to the point cloud location, so the grouped points in each voxel are represented as point features. There are two deformable feature learning layers with each layer having 2 subgraphs with 16-dimensional outputs. Note that the voxel partition is based on the original point cloud location. Then as VoxelNet, the point features in each voxel are fed to 2 voxel feature encoding layers with channel 32 and 128 to get sparse 4D tensors representing the space. The convolutional middle layers process 4D tensors to further aggregate spatial context. Finally a RPN generates the 3D detection.

We report the performance of 3 networks: (1) VoxelNet baseline [34]; (2) our fixed graph baseline, where we used the original point cloud location to learn the point feature at the place of spatial transformer blocks; (3) deformable spatial transformer networks as discussed above.

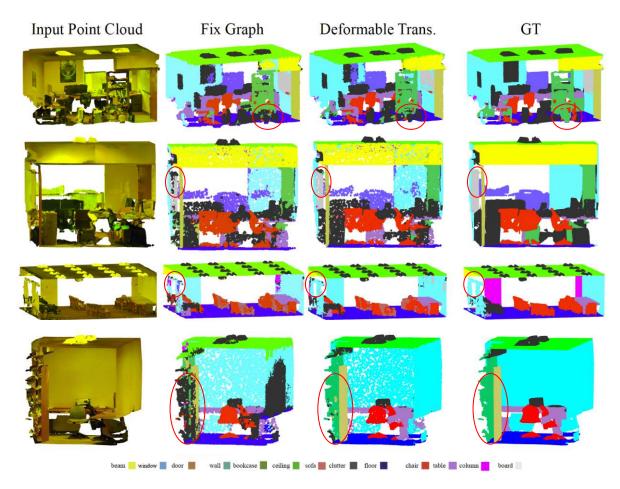


Fig. 9. **Qualitative results for semantic segmentation** of our deformable spatial transformer and the fix graph baseline. The first column is the input point cloud, the second and the third column shows the fix graph and our spatial transformer results, and the last column is the ground truth. Points belonging to different semantic regions are colored differently. We observe better and more consistent segmentation result with our spatial transformer, specifically for the areas circled in red.

Result and analysis. Table 4.3 reports car detection results on KITTI validation set.¹ Compared with baseline, having a point feature learning module improves the performance by 7.3% and 2.8% for birds' eye view and 3D detection performance on average, respectively. The deformable module further improves 8.9% and 3.9%, respectively, on birds' eye view and 3D detection performance on average, compared with the VoxelNet baseline. We observe performance boost with our deformable spatial transformer.

TABLE 5
Performance of different number of deformable transformation modules.

Metric is average mIOU (%).

	fixed graph	1 graph	2 graphs	4 graphs
$f_i^{(t)} = 32$	84.2	84.9	85.2	85.3
$f_i^{(t)} k_i^{(t)} = 64$	84.2	85.3	85.2	83.5

In the first row, the output feature of each sub-graph is of dim. 32, while the number of subgraphs changes; the second row limits the multiplication of number of sub-graphs and sub-feature dim. to be 64.

4.5 Ablation Studies

We conduct ablation studies to understand how many spatial transformers may be sufficient to achieve satisfactory performance. As our deformable spatial transformers consist of two parts: transformations of point coordinates and features, we also conduct ablation studies to understand the function of each part.

Influence of the number of spatial transformers. Table 5 shows the performance of different number of deformable spatial transformers. When sub-feature dimension is fixed, the more graphs in each layer, the higher the performance.

1. As the authors of the paper did not provide code, we use the third party implemented code [39] and obtain lower performance than that reported in the original paper.

With the limited resources (the multiplication of number of sub-graphs and sub-feature dimension to be 64), the best performance is achieved at k=1, f=64 and k=2, f=32

Influence of different components in deformable spatial transformer. As in Equation 7, the deformable spatial transformer consists of two components: affine transformation on point location, AP, and three-dimensional projection of high-dimensional feature, CF. Fig. 8 depicts performance of different component of deformable transformation learning module. We observe average mIOU improvement of both affine and feature only spatial transformer, while deformable spatial transformer (the combination of both) gives the highest performance boost.

4.6 Time and Space Complexity

Table 6 shows that with the same model size and almost the same test time, the significant performance gain can be achieved. We increase the number of channel in the fixed graph baseline model for all experiments for fair comparison. Note that even without increasing number of parameters of baseline, adding spatial transformer only increases number of parameters by 0.1%, as number of parameters of transformation matrix is very small.

TABLE 6 Model size and test time on ShapeNet part segmentation.

	SpaltNet [29]	[29] + Spatial Transformer
# Params.	2, 738K	2, 738K
Test time (s/shape)	0.352	0.379

4.7 Visualization and Analysis

We illustrate the merits of the proposed spatial transformers by visualizing the global and local view of the transformed 3D points. We also visualize the changes in local patches when applying spatial transformers.

Global view of the deformable transformation. Fig. 10 depicts some examples of learned deformable transformation in ShapeNet part segmentation. We observe that each graph at certain layer aligns input 3D shape with similar semantic geometric transformation. For example, regardless the shape of the rocket, graph 2 at layer 2 always capture the rocket wing information.

Local view of the deformable transformation. Point cloud data is not usually balanced sampled, which makes point cloud convolution challenging, as the k-NN graph does not accurately represents the exact neighborhood and 3D structure information. Our deformable spatial transformer can gives every point flexibility and in turn can capture better affinity matrix and find better local patches, but can it implicitly make the point cloud closer to balanced sampling?

Fig. 11 shows the local view of a sample of skateboard after deformable transformations, the points are deformed to be more uniformly distributed. We also analyze the standard deviation of data and transformed point clouds in the ShapeNet dataset. The standard deviation of point clouds decreases 50.2% over all categories when applied spatial transformers. (We normalize the point coordinates for fair comparison.) The decrease accounts for the more balanced sampling distribution of the transformed points.

To verify if the point cloud coordinates are statistically different after applying spatial transformers, we conduct the t-test on the original and transformed point clouds. The t-score is 7.15 overall categories with p-vale smaller than 1e-9. Applying spatial transformers therefore makes statistical difference.

Dynamic neighborhood visualization. To illustrate how our spatial transformers learn diverse neighborhoods for 3D shapes, we show the nearest neighbors of two query points and use corresponding colors to indicate corresponding neighborhoods. **(1)** As in in Fig. 12, neighborhoods retrieved from deformed shape encode additional semantic information, compared to neighborhoods from 3D coordinates.

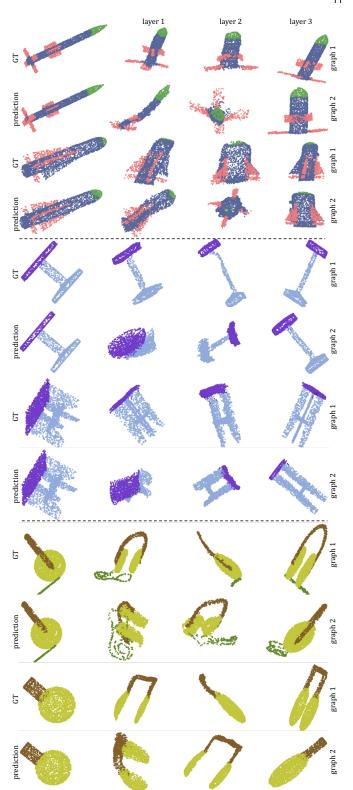


Fig. 10. **Examples of learned deformable transformations** in ShapeNet part segmentation. 3D shapes include rocket, table and earphone (from up to bottom). We observe that each graph at certain layer aligns input 3D shape with similar semantic geometric transformation, e.g., graph 2 (2) at layer 2 (1) in rocket (table) example captures the wing (table surface) information.

(2) As shown in additional graph visualizations (Fig. 2) of table and earphone, different graphs enable the ability of

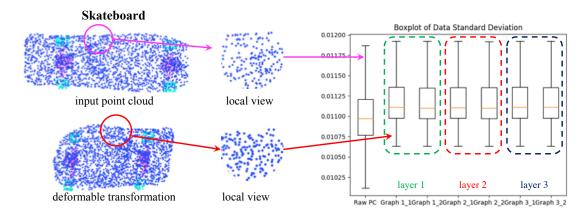


Fig. 11. Local view of transformed points with spatial transformer. Deformable spatial transformer makes the point cloud closer to balanced sampling, and makes nearest-neighbor-based local patch grouping and point cloud feature learning more efficient.

the network to learn from diverse neighborhoods without incurring additional computational burden.

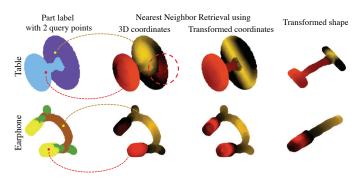


Fig. 12. **Nearest neighbor retrieval** of two query points (red and yellow) using (transformed) 3D coordinates. Rotating version. Neighborhood of the transformed coordinates encode additional semantic information: the neighborhood inside the dashed circle changes to adapt to table base part.

5 CONCLUSION

In this work, we propose novel spatial transformers for 3D point clouds, which can be easily added to existing point cloud processing networks. The spatial transformers can alter local point neighborhoods for efficient feature learning for different point cloud processing tasks.

We first analyze different transformations and their influence on affinity matrix and local point neighborhood. We further proposed one linear (affine) spatial transformer and two non-linear (projective and deformable) spatial transformers. We demonstrate how spatial transformers can achieve more efficient feature learning with dynamic local neighborhoods in a point cloud processing network.

We evaluate the performance of the proposed spatial transformer on two types of point cloud networks (point-based [22], [23] and sampling-based [29] method) on three large-scale 3D point cloud processing tasks (part segmentation, semantic segmentation and detection). Our spatial transformers also achieved superior performance than its fix graph counterpart for state-of-the-art methods.

Although successful, our deformable spatial transformers do not have many constraints to cope with the geometric information of the 3D shape. Future work could design better non-linear spatial transformers for point cloud. On the other hand, spatial transformers focus on learning transformations of the global 3D shape and altering local neighborhoods for more efficient feature learning. Future works could also explore how local transformations help with feature learning for 3D point clouds.

REFERENCES

- [1] C.-H. Lin, Y. Chung, B.-Y. Chou, H.-Y. Chen, and C.-Y. Tsai, "A novel campus navigation app with augmented reality and deep learning," in 2018 IEEE International Conference on Applied System Invention (ICASI). IEEE, 2018, pp. 1075–1077.
- [2] J. R. Rambach, A. Tewari, A. Pagani, and D. Stricker, "Learning to fuse: A deep learning approach to visual-inertial camera pose estimation," in *Mixed and Augmented Reality (ISMAR)*, 2016 IEEE International Symposium on. IEEE, 2016, pp. 71–76.
- [3] S. Tulsiani, S. Gupta, D. Fouhey, A. A. Efros, and J. Malik, "Factoring shape, pose, and layout from the 2d image of a 3d scene," in *Proceedings of the IEEE Conference on Computer Vision and Pattern Recognition*, 2018, pp. 302–310.
- [4] S. Vasu, M. M. MR, and A. Rajagopalan, "Occlusion-aware rolling shutter rectification of 3d scenes," in *Proceedings of the IEEE Conference on Computer Vision and Pattern Recognition*, 2018, pp. 636–645.
- [5] A. Dai, D. Ritchie, M. Bokeloh, S. Reed, J. Sturm, and M. Nießner, "Scancomplete: Large-scale scene completion and semantic segmentation for 3d scans," in CVPR, vol. 1, 2018, p. 2.
- [6] Y. Chen, J. Wang, J. Li, C. Lu, Z. Luo, H. Xue, and C. Wang, "Lidar-video driving dataset: Learning driving policies effectively," in Proceedings of the IEEE Conference on Computer Vision and Pattern Recognition, 2018, pp. 5870–5878.
- [7] S. Shen, "Stereo vision-based semantic 3d object and ego-motion tracking for autonomous driving," arXiv preprint arXiv:1807.02062, 2018.
- [8] B. Wu, A. Wan, X. Yue, and K. Keutzer, "Squeezeseg: Convolutional neural nets with recurrent crf for real-time road-object segmentation from 3d lidar point cloud," in 2018 IEEE International Conference on Robotics and Automation (ICRA). IEEE, 2018, pp. 1887–1893.
- [9] J. Deng, W. Dong, R. Socher, L.-J. Li, K. Li, and L. Fei-Fei, "Imagenet: A large-scale hierarchical image database," in 2009 IEEE conference on computer vision and pattern recognition. Ieee, 2009, pp. 248–255.
- [10] A. Krizhevsky, I. Sutskever, and G. E. Hinton, "Imagenet classification with deep convolutional neural networks," in *Advances in neural information processing systems*, 2012, pp. 1097–1105.
- [11] Z. Wu, S. Song, A. Khosla, F. Yu, L. Zhang, X. Tang, and J. Xiao, "3d shapenets: A deep representation for volumetric shapes," in *Proceedings of the IEEE conference on computer vision and pattern recognition*, 2015, pp. 1912–1920.
- [12] G. Riegler, A. O. Ulusoy, and A. Geiger, "Octnet: Learning deep 3d representations at high resolutions," in *Proceedings of the IEEE Conference on Computer Vision and Pattern Recognition*, vol. 3, 2017.

- [13] P.-S. Wang, Y. Liu, Y.-X. Guo, C.-Y. Sun, and X. Tong, "O-cnn: Octree-based convolutional neural networks for 3d shape analysis," ACM Transactions on Graphics (TOG), vol. 36, no. 4, p. 72, 2017.
- [14] H. Su, S. Maji, E. Kalogerakis, and E. Learned-Miller, "Multiview convolutional neural networks for 3d shape recognition," in *Proceedings of the IEEE international conference on computer vision*, 2015, pp. 945–953.
- [15] C. R. Qi, H. Su, M. Nießner, A. Dai, M. Yan, and L. J. Guibas, "Volumetric and multi-view cnns for object classification on 3d data," in *Proceedings of the IEEE conference on computer vision and* pattern recognition, 2016, pp. 5648–5656.
- [16] E. Kalogerakis, M. Averkiou, S. Maji, and S. Chaudhuri, "3d shape segmentation with projective convolutional networks," in *Proc.* CVPR, vol. 1, no. 2, 2017, p. 8.
- [17] L. Zhou, S. Zhu, Z. Luo, T. Shen, R. Zhang, M. Zhen, T. Fang, and L. Quan, "Learning and matching multi-view descriptors for registration of point clouds," arXiv preprint arXiv:1807.05653, 2018.
 [18] C. R. Qi, H. Su, K. Mo, and L. J. Guibas, "Pointnet: Deep learning on
- [18] C. R. Qi, H. Su, K. Mo, and L. J. Guibas, "Pointnet: Deep learning on point sets for 3d classification and segmentation," *Proc. Computer Vision and Pattern Recognition (CVPR)*, IEEE, vol. 1, no. 2, p. 4, 2017.
- [19] C. R. Qi, L. Yi, H. Su, and L. J. Guibas, "Pointnet++: Deep hierarchical feature learning on point sets in a metric space," in Advances in Neural Information Processing Systems, 2017, pp. 5099– 5108.
- [20] D. Rethage, J. Wald, J. Sturm, N. Navab, and F. Tombari, "Fully-convolutional point networks for large-scale point clouds," arXiv preprint arXiv:1808.06840, 2018.
- [21] M. Gadelha, R. Wang, and S. Maji, "Multiresolution tree networks for 3d point cloud processing," arXiv preprint arXiv:1807.03520, 2018.
- [22] Y. Wang, Y. Sun, Z. Liu, S. E. Sarma, M. M. Bronstein, and J. M. Solomon, "Dynamic graph cnn for learning on point clouds," arXiv preprint arXiv:1801.07829, 2018.
- [23] Y. Li, R. Bu, M. Sun, W. Wu, X. Di, and B. Chen, "Pointcnn: Convolution on x-transformed points," in *Advances in Neural Information Processing Systems*, 2018, pp. 820–830.
- [24] Y. Feng, Z. Zhang, X. Zhao, R. Ji, and Y. Gao, "Gvcnn: Groupview convolutional neural networks for 3d shape recognition," in *Proceedings of the IEEE Conference on Computer Vision and Pattern Recognition*, 2018, pp. 264–272.
- [25] Z. Han, M. Shang, Z. Liu, C.-M. Vong, Y.-S. Liu, M. Zwicker, J. Han, and C. P. Chen, "Seqviews2seqlabels: Learning 3d global features via aggregating sequential views by rnn with attention," *IEEE Transactions on Image Processing*, vol. 28, no. 2, pp. 658–672, 2019.
- [26] D. Maturana and S. Scherer, "Voxnet: A 3d convolutional neural network for real-time object recognition," in 2015 IEEE/RSJ International Conference on Intelligent Robots and Systems (IROS). IEEE, 2015, pp. 922–928.
- [27] M. Tatarchenko, A. Dosovitskiy, and T. Brox, "Octree generating networks: Efficient convolutional architectures for high-resolution 3d outputs," in *Proceedings of the IEEE International Conference on Computer Vision*, 2017, pp. 2088–2096.
- [28] R. Klokov and V. Lempitsky, "Escape from cells: Deep kd-networks for the recognition of 3d point cloud models," in *Proceedings of the* IEEE International Conference on Computer Vision, 2017, pp. 863–872.
- [29] H. Su, V. Jampani, D. Sun, S. Maji, E. Kalogerakis, M.-H. Yang, and J. Kautz, "Splatnet: Sparse lattice networks for point cloud processing," in *Proceedings of the IEEE Conference on Computer Vision* and Pattern Recognition, 2018, pp. 2530–2539.
- [30] A. Adams, J. Baek, and M. A. Davis, "Fast high-dimensional filtering using the permutohedral lattice," in *Computer Graphics Forum*, vol. 29, no. 2. Wiley Online Library, 2010, pp. 753–762.
- [31] V. Jampani, M. Kiefel, and P. V. Gehler, "Learning sparse high dimensional filters: Image filtering, dense crfs and bilateral neural networks," in *Proceedings of the IEEE Conference on Computer Vision* and Pattern Recognition, 2016, pp. 4452–4461.
- [32] L. Landrieu and M. Simonovsky, "Large-scale point cloud semantic segmentation with superpoint graphs," in *Proceedings of the IEEE Conference on Computer Vision and Pattern Recognition*, 2018, pp. 4558–4567.
- [33] J. Li, B. M. Chen, and G. Hee Lee, "So-net: Self-organizing network for point cloud analysis," in *Proceedings of the IEEE conference on computer vision and pattern recognition*, 2018, pp. 9397–9406.
- [34] Y. Zhou and O. Tuzel, "Voxelnet: End-to-end learning for point cloud based 3d object detection," in *Proceedings of the IEEE Conference on Computer Vision and Pattern Recognition*, 2018, pp. 4490–4499.

- [35] J. Dai, H. Qi, Y. Xiong, Y. Li, G. Zhang, H. Hu, and Y. Wei, "Deformable convolutional networks," *CoRR*, abs/1703.06211, vol. 1, no. 2, p. 3, 2017.
- [36] A. X. Chang, T. Funkhouser, L. Guibas, P. Hanrahan, Q. Huang, Z. Li, S. Savarese, M. Savva, S. Song, H. Su et al., "Shapenet: An information-rich 3d model repository," arXiv preprint arXiv:1512.03012, 2015.
- [37] I. Armeni, O. Sener, A. R. Zamir, H. Jiang, I. Brilakis, M. Fischer, and S. Savarese, "3d semantic parsing of large-scale indoor spaces," in *Proceedings of the IEEE Conference on Computer Vision and Pattern Recognition*, 2016, pp. 1534–1543.
- [38] A. Geiger, P. Lenz, and R. Urtasun, "Are we ready for autonomous driving? the kitti vision benchmark suite," in 2012 IEEE Conference on Computer Vision and Pattern Recognition. IEEE, 2012, pp. 3354– 3361.
- [39] Q. Huang, "Voxelnet: End-to-end learning for point cloud based 3d object detection - code," https://github.com/qianguih/voxelnet, 2019